Cell PRESS
Structure
Article

Reconstruction of the $P2X_2$ Receptor Reveals a Vase-Shaped Structure with Lateral Tunnels above the Membrane

Kazuhiro Mio,[1,2,9] Toshihiko Ogura,[1,3,9] Tomomi Yamamoto,[4] Yoko Hiroaki,[5,6] Yoshinori Fujiyoshi,[2,6,7] Yoshihiro Kubo,[4,8,*] and Chikara Sato[1,2,*]

[1]Neuroscience Research Institute, National Institute of Advanced Industrial Science and Technology, Umezono 1-1-4, Tsukuba, Ibaraki 305-8568, Japan
[2]Biomedicinal Information Research Center, National Institute of Advanced Industrial Science and Technology, 2-41-6 Aomi, Koto-ku, Tokyo 135-0064, Japan
[3]PRESTO, Japan Science and Technology Agency, 4-1-8 Honcho Kawaguchi, Saitama 332-0012, Japan
[4]Division of Biophysics and Neurobiology, Department of Molecular Physiology, National Institute for Physiological Sciences, Myodaiji, Okazaki, Aichi 444-8585, Japan
[5]Japan Biological Informatics Consortium, Oiwake, Kitashirakawa, Sakyo-ku, Kyoto 606-8502, Japan
[6]Department of Biophysics, Graduate School of Science, Kyoto University, Oiwake, Kitashirakawa, Sakyo-ku, Kyoto 606-8502, Japan
[7]CREST
[8]SORST
Japan Science and Technology Agency, 4-1-8 Honcho Kawaguchi, Saitama 332-0012, Japan
[9]These authors contributed equally to this work
*Correspondence: ykubo@nips.ac.jp (Y.K.), ti-sato@aist.go.jp (C.S.)
DOI 10.1016/j.str.2008.12.007

SUMMARY

In response to the intercellular messenger ATP, P2X receptors transfer various sensory information, including pain. Here we have reconstructed the structure of the $P2X_2$ receptor at 15 Å resolution from more than 90,000 particle images, taken with a cryo-electron microscope equipped with a helium-cooled stage. This three-dimensional depiction, presumably in a closed state, revealed an elongated vase-shaped structure 202 Å in height and 160 Å in major diameter. The extracellular and transmembrane domains present a two-layered structure, in which a sparse outer layer surrounds a pore-forming inner density. The decreased diameter of a putative ion-conducting pathway at the middle of the membrane was considered to be the narrowest part of the pore, which has been predicted from electrophysiological studies. The sparse, extended structure of the $P2X_2$ receptor indicates a loose assembly of subunits, which could be a basis for the activation-dependent pore dilation of P2X receptors.

INTRODUCTION

Extracellular adenosine 5′-triphosphate (ATP) acts as a neurotransmitter which stimulates nearby cells to induce various biological functions. It is received by two different types of cell-surface receptors, the P2X and P2Y families (Burnstock, 2007). P2Xs are ATP-gated cation-permeable ion channels, whereas P2Ys are G protein-coupled receptors. To date, seven types of P2X receptors and eight types of P2Y receptors have been identified in the human genome.

P2X receptors are widely distributed both in the peripheral and the central nervous systems, where they play critical roles in fast synaptic transmissions and in presynaptic modulations (Brake et al., 1994; Valera et al., 1994; Khakh, 2001; North, 2002; Burnstock, 2007). The sensation of pain is the most extensively studied function of P2X receptors. The $P2X_{2/3}$ channel is a heteromeric trimer of highly homologous $P2X_2$ and $P2X_3$ subunits, and evokes impulses in sensory pathways when it receives ATP from damaged tissue (Chen et al., 1995; Lewis et al., 1995). Neurons from $P2X_2$/$P2X_3$ double knockout mice had minimal or no response to ATP, and the mice lacked taste responses but remained sensitive to touch, temperature, and menthol (Cockayne et al., 2005; Finger et al., 2005). Activation of the $P2X_4$ receptor in hyperactive microglia due to nerve injury causes tactile allodynia, whereas pharmacological blocking of the $P2X_4$ receptor relieves pain (Tsuda et al., 2003). Recent studies reported involvement of the P2X receptor in much wider physiological functions, including taste transmission (Finger et al., 2005), sound transduction (Aubert et al., 1994), control of breathing in oxygen-depressed brain (Gourine et al., 2005), and neuronal injury including ischemia/hypoxia and trauma/axotomy (Florenzano et al., 2002; Cavaliere et al., 2003).

In spite of a homology in sequence within the family, ATP desensitization kinetics are quite different; desensitization is fast for $P2X_1$ and $P2X_3$, slow for $P2X_2$ and $P2X_4$, and no desensitization is recorded for $P2X_7$ (North, 2002). After exposure to ATP for longer periods or at high doses, P2X receptors permeate previously impermeable large cations such as N-methyl-D-glucamine in a time- and dose-dependent manner. This pore dilation in P2X receptors (Khakh et al., 1999; Virginio et al., 1999; Eickhorst et al., 2002) is reported to be dependent on the density of P2X receptors on the plasma membrane (Fujiwara and Kubo, 2004).

In spite of the unique gating properties and the clinical importance of P2X receptors, structural information about them is quite limited. Atomic force microscopy has provided low-resolution

images of the trilaterally (C3) symmetrical $P2X_2$ receptor (Barrera et al., 2005) and further hypothesized an ATP-induced $P2X_2$ subunit association (Nakazawa et al., 2005). Our previous study using negatively stained electron microscopy (EM) and statistical analysis clearly provided direct visual images of C3 symmetric top projections and averaged images of the $P2X_2$ receptor (Mio et al., 2005). However, the resolution of each class average was limited due to deformation by dryness and uneven staining which prevented us from applying the three-dimensional reconstruction technique (van Heel et al., 2000; Rosenthal and Henderson, 2003; Frank, 2006). In this study, we have recorded the projections of the $P2X_2$ protein using cryo-EM equipped with a helium-cooled stage (Fujiyoshi et al., 1991) under ATP-free conditions, and reconstructed the 3D structure at 15 Å resolution from 90,146 automatically selected particles.

RESULTS

Characterization and Purification of Heterologously Expressed $P2X_2$ Protein

We first constructed a baculovirus containing rat $P2X_2$ cDNA tagged with a FLAG sequence at either the N or C terminus (abbreviated N- or C-FLAG $P2X_2$), and infected Sf9 cells with the recombinant virus. The expressed N- and C-FLAG $P2X_2$ proteins were correctly localized on the plasma membrane, and shown to be fully glycosylated and functionally equivalent to wild-type $P2X_2$ by electrophysiological analyses using *Xenopus* oocytes (Mio et al., 2005 and unpublished data). Preliminary EM observations confirmed that these proteins are uniformly packed and almost identical to each other. However, the yield of C-FLAG $P2X_2$ was 60% that of N-FLAG $P2X_2$, and we have chosen N-FLAG $P2X_2$ for the following studies.

$P2X_2$ protein was solubilized from the cell membrane using *n*-dodecyl β-D-maltoside (DDM) and purified in two steps: anti-FLAG-immunoaffinity chromatography and size-exclusion chromatography (SEC) (Mio et al., 2005). SDS-PAGE analysis and western blotting using anti-FLAG antibody demonstrated that a major band at approximately 70 kDa is N-FLAG $P2X_2$ protein, with the peak at fraction number 3 (Figure 1A). The observed size on the gel is much larger than the estimation from the amino acid sequence (53.7 kDa including FLAG tag), reflecting a higher level of glycosylation (Newbolt et al., 1998; Torres et al., 1998).

Although we have selected the most suitable detergent for solubilizing $P2X_2$ protein from the membrane and conducted the experiments carefully, minor contamination of monomeric $P2X_2$ remained in the affinity-purified specimen. To remove these monomer peptides as well as other contaminants and degraded $P2X_2$ protein, we further applied Superdex 200 SEC as the second step of purification to the specimen. The elution of protein by SEC was analyzed by UV absorbance at 280 nm (Figure 1B, upper) and by SDS-PAGE followed by silver staining (Figure 1B, lower). $P2X_2$ protein was eluted as a main peak at 1.12 ml, as shown by the intensity of the bands in the gel. UV absorption at 0.87 ml elution was not accompanied by detectable proteins (data not shown), which is speculated to be due to micelles of detergents and/or lipids. Minor peaks eluting between 1.12 and 1.96 ml include degraded and/or deglycosylated $P2X_2$ protein and other contaminants as observed in Figure 1A, while a peak at 1.96 ml contains FLAG peptides used to elute $P2X_2$ protein. The crosslinking experiments represent that the affinity-purified specimen is a mixture of the monomer, dimer, and trimer $P2X_2$ protein (Figure 1C, left). After SEC, the ratio of trimer $P2X_2$ in the fraction at 1.12 ml is significantly increased (Figure 1C, right). The purity of $P2X_2$ protein in this fraction was confirmed to be more than 95% by silver staining (Figure 1B), and this fraction was used for EM study. By using this system, we obtained 8.6 μg purified $P2X_2$ protein per 1 g cells in wet volume (corresponding to the cells in a 901 cm^2 culture dish area).

The hydrated size (Stokes radius; *Rs*) of the $P2X_2$ receptor was calculated from a calibration curve using size standards in the SEC. The $P2X_2$ protein was eluted between thyroglobulin (*Rs* ≈ 85.0 Å) and ferritin (*Rs* ≈ 61.0 Å), and its *Rs* was determined to be 64.6 ± 0.52 Å (mean ± SD, n = 3) (Figure 1D).

Cryo-Electron Microscopy and 3D Reconstruction

Images of $P2X_2$ protein were recorded using a JEOL JEM3000SFF cryo-electron microscope equipped with a superfluid helium stage, which reduces irradiation damage to the specimen (Fujiyoshi et al., 1991). The images were recorded at 300 kV acceleration voltage. The use of the helium-cooled stage and a higher acceleration voltage in EM recording potentially increases the resolution of the images, although their contrast decreases. The particles recorded under these conditions were faintly observed as triangular or polygonal objects in the noisy raw images; their dimensions are comparable to a scale bar of 200 Å (Figure 1E). In general, reduced contrast of EM images makes particle pickup difficult. However, our automated particle pickup systems were shown to be able to easily select the particle images, even in those noisy images. The $P2X_2$ particles were picked up by a combination of two automatic programs: the autoaccumulation method using SA (Ogura and Sato, 2004a) and the three-layered neural network method (Ogura and Sato, 2001, 2004b), and the 3D structure was reconstructed with echo-correlated reconstruction methods using SA assuming C3 symmetry in our *s*ingle-*p*article *i*mage analysis method using *n*eural *n*etwork and *s*imulated annealing (SPINNS) (Yazawa et al., 2007) and other algorithms in the IMAGIC V software (van Heel et al., 1996) (see Experimental Procedures for details). Because negatively stained EM indicated the significantly sparse structure of the $P2X_2$ receptor (Mio et al., 2005), we selected a large number of projections (90,146) from the digitized EM films to improve resolution. The final reconstruction included 46,511 particles, 51.6% of all the selected images.

In spite of large divergence in the shapes of the raw images (Figure 2A, first row), they are consistent in size, shape, and inner structures with their corresponding class averages (second row) and with the surface representations and reprojections of the reconstructed 3D structure (third and fourth rows), indicating successful 3D reconstruction. A plot of the Euler angles of the 177 class averages adopted shows that the $P2X_2$ receptor is essentially randomly oriented in the frozen buffer layer (Figure 2B). According to the Fourier shell correlation (FSC) function, the resolution of our final density map is 15.4 Å at the point of intersection with the 3σ noise curve, and 22.0 Å by the FSC > 0.5 criterion (Figure 2C). Because of the absence of ligands in the specimen, the reconstructed structure is assumed to be of the closed state.

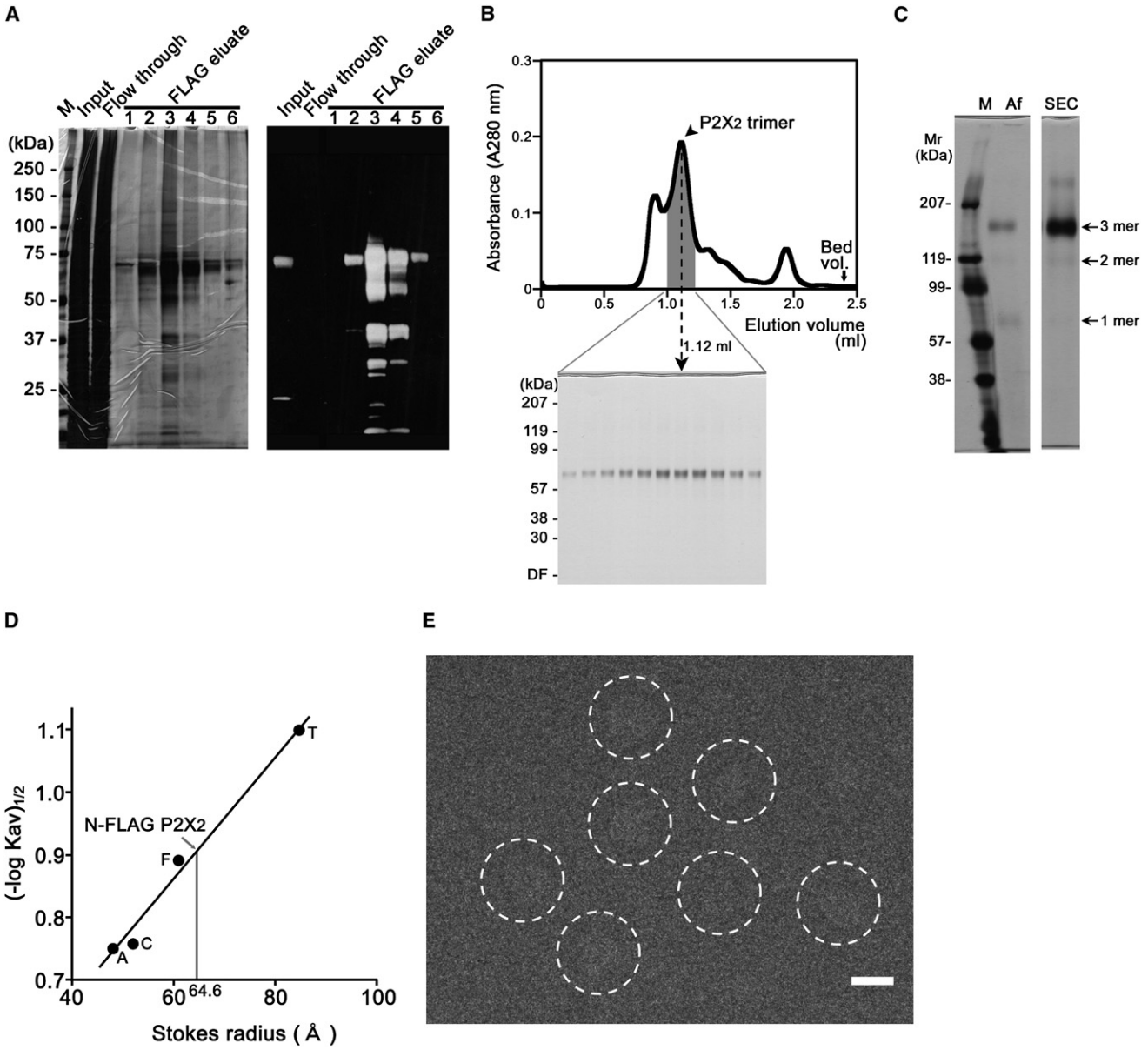

Figure 1. Purification and Cryo-EM of the Recombinant $P2X_2$ Receptor

FLAG-tagged $P2X_2$ protein was heterologously expressed in Sf9 cells, solubilized from the membrane using *n*-dodecyl β-D-maltoside (DDM), and purified by FLAG-affinity chromatography and size-exclusion chromatography (SEC).

(A) SDS-PAGE at each purification step in FLAG-affinity chromatography, visualized by silver staining (left) or western blotting using anti-FLAG antibody (right). The main band at 70 kDa represents N-FLAG $P2X_2$ protein, although degraded fragments are also observed. M, molecular standards.

(B) $P2X_2$ protein-rich eluates from the affinity column were pooled, concentrated, and further purified by Superdex 200 SEC. The elution of protein was analyzed by UV absorption at 280 nm (upper) and by SDS-PAGE followed by silver staining (lower). The purity of the $P2X_2$ protein in the peak fraction at 1.12 ml was confirmed to be more than 95% (dotted arrow), and this fraction was used for EM.

(C) Chemical crosslinking of $P2X_2$ protein after anti-FLAG-affinity chromatography (Af) and subsequent SEC (SEC). Samples were treated with 5 mM glutaraldehyde, separated by SDS-PAGE, and visualized by silver staining. Positions of the monomer, dimer, and trimer are indicated. Note that crosslinked protein moves slightly faster than untreated protein.

(D) The Stokes radius (*Rs*) of the $P2X_2$ receptor was calculated to be 64.6 ± 0.52 Å (mean ± SD, n = 3) from the elution volumes of the $P2X_2$ receptor and the standards. A, aldolase (*Rs*, 48.1 Å); C, catalase (*Rs*, 52.2 Å); F, ferritin (*Rs*, 61.0 Å); and T, thyroglobulin (*Rs*, 85.0 Å).

(E) Projections of $P2X_2$ receptors recorded using a JEOL JEM3000SFF cryo-electron microscope. They appear as triangles or elongated polygons, sparse inside but surrounded by dense boundaries (dotted circles). For statistical analysis, 334 particles were picked up by the autoaccumulation method and used to train the three-layer neural network (NN) auto-picking system, resulting in the selection of a further 92,407 particles. The scale bar represents 200 Å.

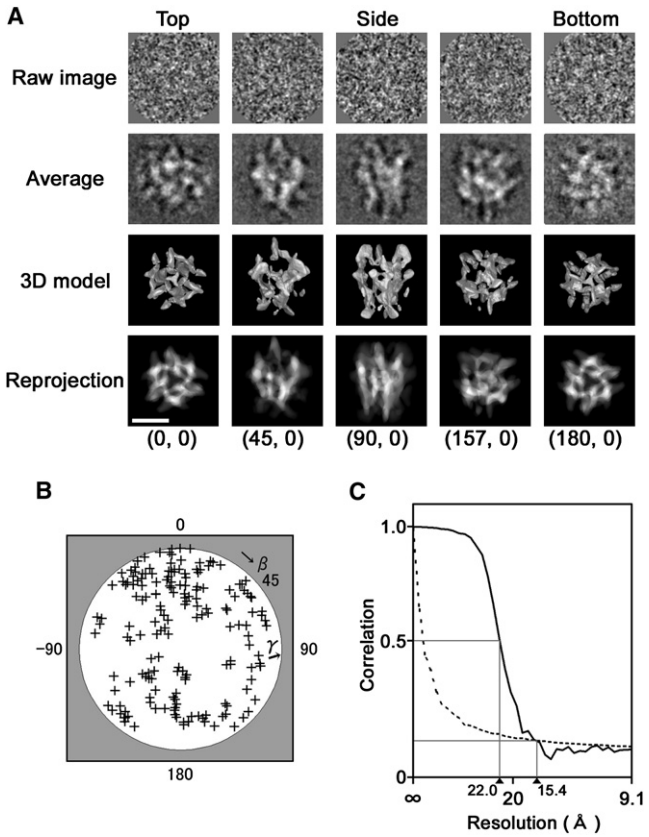

Figure 2. Three-Dimensional Reconstruction of the $P2X_2$ Receptor

(A) Raw images of $P2X_2$ protein with different Euler angles (row 1) are compared with the corresponding 2D averages (row 2), and with the surface views and reprojections of the 3D reconstruction (rows 3 and 4), consistent through the reconstruction. Each Euler angle ($\alpha = 0$, β, γ) is denoted. The scale bar represents 100 Å.

(B) The plot of the Euler angles (β, γ) of 177 adopted class averages demonstrates almost random orientations of $P2X_2$ molecules in the frozen buffer layer.

(C) The Fourier shell correlation (FSC) function indicates the resolution limit of 15.4 Å at intersecting points between signal (solid line) and the 3σ noise curve (dashed line), or 22.0 Å by the FSC > 0.5 criterion.

The resolution limit in this reconstruction is slightly lower than that of the recently reconstructed TRPC3 channel, which represents a 15.3 Å resolution limit by the FSC > 0.5 criterion (Mio et al., 2007). The $P2X_2$ receptor is constituted of thin fin-shaped loops whereas TRPC3 is built of slender tubes, and these structural differences may influence the microvibration inside the molecule, and consequently the resolution limit.

Determination of Membrane Topology

Three asparagine residues at the extracellular loop (N182, N239, and N298 in rat $P2X_2$) are potential glycosylation sites (Brake et al., 1994) (Figure 3A), which can be labeled with specific lectins. To assign the extracellular loop using lectin labeling and EM, we first examined specificities of lectins against the $P2X_2$ molecule by the lectin western blotting technique. Among seven lectins tested, four lectins (concanavalin A [ConA], wheat germ agglutinin [WGA], dolichos biflorus agglutinin, and soybean agglutinin) recognized the $P2X_2$ protein. Figure 3B shows that both ConA and WGA detected only intact $P2X_2$ protein and did not react with the PNGase F-treated sample, suggesting a mixed sugar component of α-linked mannose (recognized by ConA) and N-acetyl glucosamine (recognized by WGA) on the extracellular surface. A band at 36 kDa in PNGase F-treated lanes is the applied enzyme protein (Figure 3B).

Gold-conjugated ConA or WGA was mixed with purified $P2X_2$ protein to form $P2X_2$/lectin-gold complexes. EM of negatively stained complexes depicts both conjugates at the larger domain of the $P2X_2$ molecule, suggesting this side locates outside the cell (Figure 3C). In spite of the large size of colloidal gold (approximately 50 Å in diameter), $P2X_2$ molecules bearing multiple golds were frequently observed, indicating that the glycosylated surface is large enough to avoid steric hindrance between the conjugates.

Because P2X receptors contain intracellular N and C termini, two hydrophobic transmembrane segments (TM-1 and TM-2), and a cysteine-rich extracellular loop (Newbolt et al., 1998; Torres et al., 1998), anti-FLAG antibody was used to identify the cytoplasmic N terminus of the $P2X_2$ molecule. EM observation of negatively stained $P2X_2$ protein/anti-FLAG antibody complexes demonstrates that the antibodies attached to the smaller domain, confirming this side is cytoplasmic (Figure 3D, upper). This was more clearly demonstrated by the binding of its Fab fragments conjugated with colloidal gold (Figure 3D, lower). $P2X_2$'s trimeric stoichiometry allows decoration of two or three antibodies simultaneously.

Surface Representation of the $P2X_2$ Molecule

The 3D structure of the $P2X_2$ receptor was reconstructed from the class averages of a wide range of Euler angles (Figure 2B). It revealed an elongated vase-shaped structure 202 Å in height and 160 Å in major diameter, at 22 Å externally from the membrane (the position of the membrane is indicated by blue lines; see below) (Figure 4). The diameter decreases to 105 Å at the middle of the membrane and to 92 Å at the narrower cytoplasmic domain (Figure 4B). The top view presents a clover leaf-shaped structure with a small Y-shaped density at the center (Figure 4A). The extracellular arms extend outside the cell to outline the outer layer, and reserve a low-density funnel inside (Figure 4B). In contrast, the densities at the transmembrane and cytoplasmic domains are moderately packed: a cone-shaped density continues from the transmembrane to the cytoplasm and is followed by a tripod extension. They are slightly twisted around the symmetry axis. Large splits and orifices are laterally opening toward outside the molecule at both the extracellular and cytoplasmic domains (Figure 4B). Because the density of glycan is similar to that of protein ($d = 1.37$ g/cm^3), the final volume is assumed to include both the $P2X_2$ peptide and the glycan moiety. The presented isosurfaces (Figure 2, row 3; Figure 4) contain 155% of the molecular mass for trimer peptides and glycan (209 kDa).

Hydropathy analysis of the amino acid sequence suggests that the 3D volumes of extracellular, transmembrane, and cytoplasmic domains are 64.5%, 8.5%, and 27.0%, respectively (Figure 3A). The position of the membrane was predicted so that a membrane of 30 Å thickness separates the 3D volume to fit this ratio (Figures 4B and 5A, blue lines). The membrane divides the molecular height of 202 Å into 107 Å extracellular,

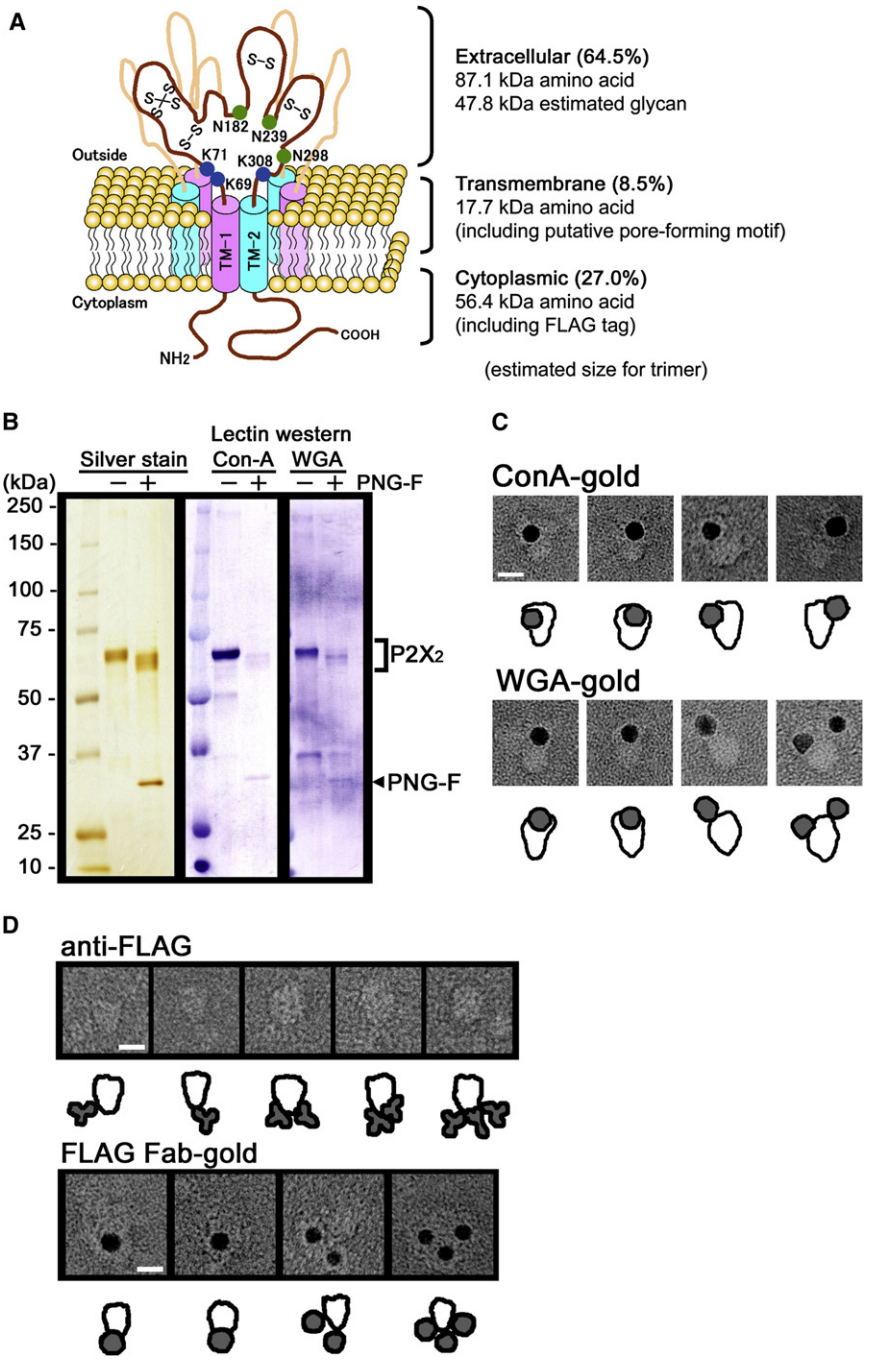

Figure 3. Assigning Domains in the $P2X_2$ Receptor

(A) Transmembrane topology predicted for the $P2X_2$ receptor. Each subunit has two transmembrane segments (TM-1 and TM-2) with an extracellular loop in which multiple disulfide bonds (S-S) constrain the structure. Three asparagine residues (N182, N239, and N298) are putative targets for glycosylation, and lysine residues proximal to the TM segments (K69, K71, and K308) interact with negatively charged ATP. The FLAG sequence (DYKDDDDK) was introduced at the N terminus for protein purification.

(B) Lectin western blotting of $P2X_2$ protein. Silver staining demonstrates that the size of the $P2X_2$ receptor is reduced by PNGase-F treatment (left). Both ConA and WGA detected intact $P2X_2$ protein, but not the PNGase-F-treated protein (middle and right).

(C) Assignment of the extracellular domain using lectin-gold. Both ConA- (upper) and WGA-gold (lower) indicate the sparse wider domain of the $P2X_2$ molecule to be extracellular. Schematic diagrams of $P2X_2$ proteins (open particles) and the gold conjugates (filled in gray) are described below.

(D) The cytoplasmic domain of $P2X_2$ protein was assigned by the binding of anti-FLAG antibody (upper) or the Fab-gold conjugate (lower) to the N-terminally tagged FLAG sequence. Both the antibody and the gold conjugate (filled in gray) suggest that the narrower end of the molecule is cytoplasmic. $P2X_2$ particles bearing two or three antibodies are also observed.

The scale bars represent 100 Å.

30 Å transmembrane, and 65 Å cytoplasmic (Figure 4B) and the 3D volume into 57.1%, 18.7%, and 24.1%, respectively. Among these domains, the resultant volume at the membrane (56.5 kDa) is much larger than the prediction (17.7 kDa), suggesting the integration of a considerable amount of lipids and detergents into the hydrophobic transmembrane domain. The volume increase of 38.8 kDa at the membrane estimates the binding of ~51–76 molecules of lipid and/or detergent per single $P2X_2$ protein, calculated from the molecular mass of 511 for DDM and 760 for phosphatidylcholine as a major component of the membrane lipids. Alternatively, the integration of extracellular or cytoplasmic segments into the transmembrane domain could increase the volume.

The dimensions of the reconstructed $P2X_2$ receptor is slightly larger than its Stokes radius estimated as 64.6 Å from the SEC (Figure 1D), suggesting the large extracellular arms are sparse and flexible and less resistant to the flow in the column. The extracellular arms may play a role in transmitting signals from extracellular regulatory proteins or from neighboring subunits in the hetero-oligomeric P2X channel to control ion permeation (Khakh et al., 2000) in an expression density-dependent manner (Fujiwara and Kubo, 2004). These arms may also protect the liganded ATP from ATPases.

Internal Structure

Horizontal and vertical sections of the reconstructed $P2X_2$ receptor revealed its two-layered structure (Figures 5A and 6A). The inner layer starts as a Y-shaped density in the middle of the extracellular domain (Figure 5A, panels 6 and 7), forms an upper vestibule above the membrane (panels 8–10), and then narrows at the middle membrane (panels 11 and 12). Inside

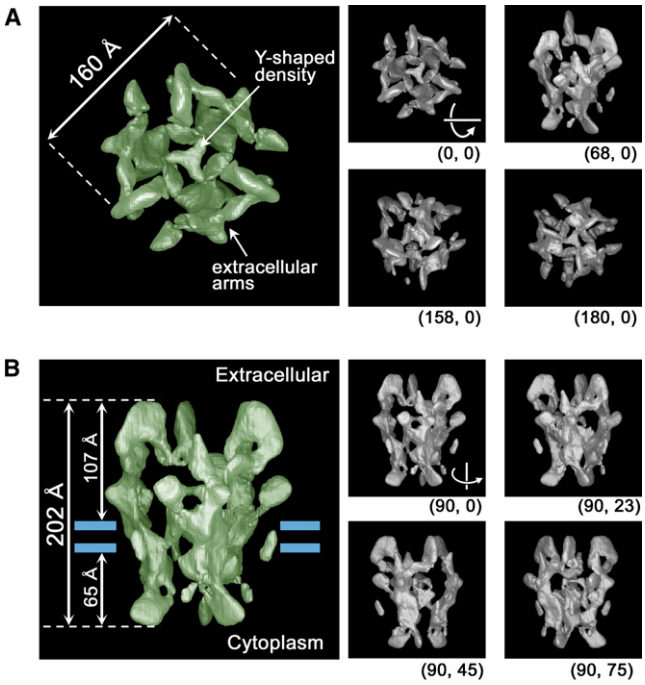

Figure 4. Surface Representation of the $P2X_2$ Protein

The $P2X_2$ receptor, presumably in a closed state, is an elongated vase-shaped molecule 202 Å in height and 160 Å in major diameter.

(A) Top view (left) and its increment rotations about the horizontal axis (right panels).

(B) Side view (left) and its rotated views about the vertical axis (right panels). Two blue lines delineate the lipid bilayer. The isosurface encloses 324.5 kDa, corresponding to 155% of the trimeric $P2X_2$ molecule with a glycan moiety of 23%. Each Euler angle ($\alpha = 0$, β, γ) is denoted.

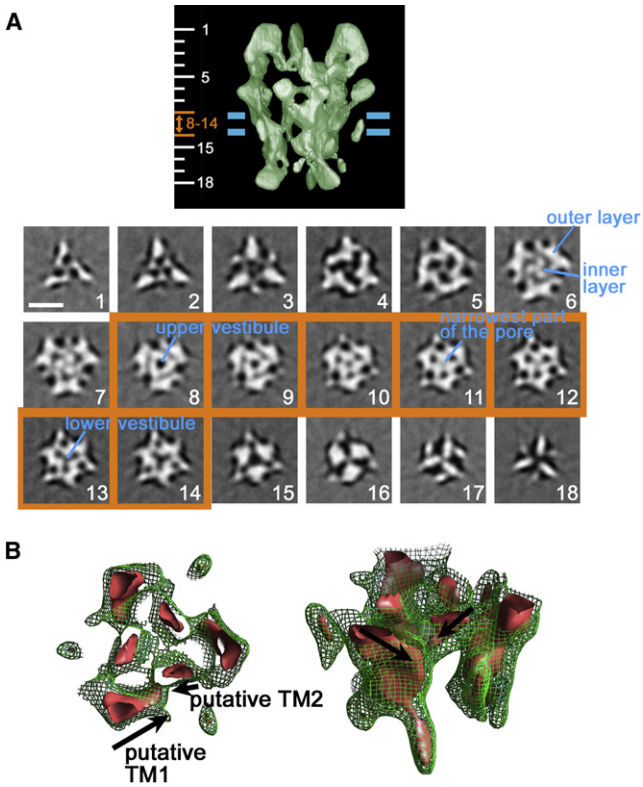

Figure 5. Horizontal Sections through the $P2X_2$ Protein

(A) Sections are displayed at 14.4 Å intervals through the extracellular (panels 1–8) and cytoplasmic (panels 14–18) domains, and at 5.0 Å intervals in the transmembrane domain (panels 8–14, framed in orange). The number of each panel corresponds to the position indicated on the upper panel. The inner layer forms upper (panels 8–10) and lower vestibules (panels 13–15). A pore located between these vestibules is narrowed at the middle of the membrane (panels 11 and 12), consistent with electrophysiological studies (Migita et al., 2001). The scale bar represents 100 Å.

(B) Structure around the transmembrane and cytoplasmic domains of the $P2X_2$ receptor viewed from the top (left) and oblique side (right), demonstrating an assembly of transmembrane segments. A green mesh denotes the isosurface enclosing a larger molecular mass of 3.9 times the trimeric $P2X_2$ receptor, and the red solid encloses a smaller molecular mass of 0.8 times. The two transmembrane segments are twisted in opposite directions to each other about the vertical axis (indicated by arrows).

the 30 Å transmembrane span, a layer 9.5 Å in thickness (panels 11 and 12) is speculated to be the narrowest part of the ion-conducting pore (Migita et al., 2001). Although the current resolution is not sufficient to determine the details of the pore structure of the P2X receptor, slightly decreased density through the central axis from the surrounding area (panel 11) suggests that the P2X receptor has an open pore structure like that of the acetylcholine receptor (AChR) (Miyazawa et al., 2003). The globular upper vestibule of 19.4 Å in width and 16.5 Å in height (Figure 5A, panels 8 and 9; Figure 6A) is separated from the low-density funnel by the Y-shaped density (Figure 6A), and connects outside of the molecule by trans-wall orifices (Figure 6B). These orifices are large enough to allow the entry of ATP and cations, but too small for extracellular ATPases.

Beneath the membrane, the inner density merges with the outer layer, forming another vestibule (Figure 5A, panels 13–15). This lower vestibule is a hemisphere of 24.3 Å in width and 24.8 Å in height, and connects to the cytoplasm laterally through three rifts between the cytoplasmic legs (Figure 5A, panels 15 and 16; Figure 6). Similar trans-wall tunnels are reported in various ion channels such as in the voltage-sensitive sodium channel (Sato et al., 2001), the Kv1.2 potassium channel (Long et al., 2005), and the AChR (Unwin, 2005). They are thought to be part of the exit pathway for permeant ions into the cytosol (Sato et al., 2001; Long et al., 2005). The basic structure around the membrane of the reconstructed $P2X_2$ receptor resembles that of other ion channels, in which a two-layered structure forms the transmembrane domain and vestibules locate at both sides of the membrane (Sato et al., 2001, 2004; Miyazawa et al., 2003).

The transmembrane segments (TM-1 and TM-2) of the $P2X_2$ subunit are separated to the outer and inner densities at the membrane (Figure 5A, panels 8–14). TM-2 is considered to constitute the inner density, because this helix is responsible for both ion permeation (Migita et al., 2001; Cao et al., 2007) and for the trimeric assembly of constituent subunits (Torres et al., 1999). Maps contoured at different thresholds demonstrate that these helices lie transverse to the membrane at different angles (Figure 5B, arrows). The outer helices (assumed to be TM-1) penetrate the membrane at 32° to the perpendicular axis to the membrane, while the inner helices (TM-2) penetrate at 23°; both locate in an antiparallel direction through the membrane. The hydrophobic space among these densities could be filled with lipids.

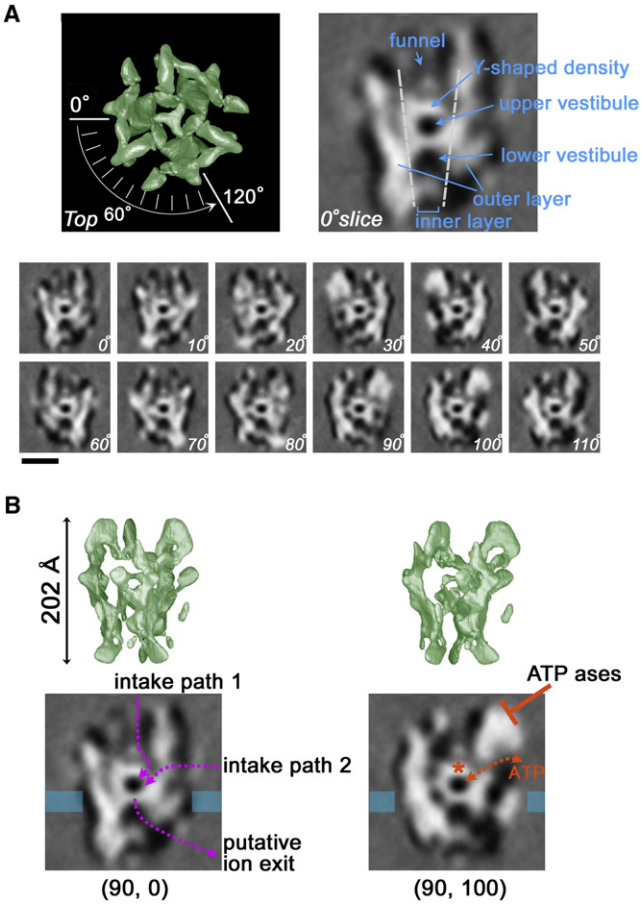

Figure 6. Vertical Sections through the $P2X_2$ Protein

(A) Gallery of sectional images along the lines every 10 degrees from 0° to 110°. Each angle is presented in the top view (upper left). The slice image at 0° (upper right) demonstrates that the Y-shaped density separates the upper vestibule (corresponding to the central hole in Figure 5A, panels 8 and 9) from the low-density funnel. The scale bar represents 100 Å.

(B) Surface representations of the $P2X_2$ receptor are viewed from two different angles with their corresponding sections. Left: in addition to a pathway from the top (intake path 1), large side openings just above the membrane (intake path 2) allow additional uptake of ATP and ions into the vestibule through small orifices on the core globe. Lateral openings in the cytoplasm are a putative exit for permeated ions. Right: the inner cover structure (asterisk), as well as the large extracellular arms, may protect liganded ATP from attack by ATPases.

DISCUSSION

Ligand-gated ion channels are composed of three major groups, namely the Cys-loop family, the ionotropic glutamate receptors, and the P2X purinergic receptors. Among them, the *Torpedo* AChR in the Cys-loop family was reconstructed at 4 Å resolution by helical reconstruction from cryo-EM images (Miyazawa et al., 2003; Unwin, 2005), and the ionotropic glutamate receptor at 21 Å resolution from recombinant protein (Tichelaar et al., 2004) and at 42 Å resolution from rat brain protein (Nakagawa et al., 2005) using single-particle analysis (resolutions using the criterion of FSC > 0.5). The structure of P2X receptors has not been clarified until recently due to difficulties in purification and crystallization, and their unusual structure.

The reconstructed $P2X_2$ receptor represents basic structural similarities to the AChR (Unwin, 2005), although AChR is a heteropentamer and its size (160 Å in height) is smaller than that of the $P2X_2$ receptor (202 Å in height). Both of them have tall, fin-shaped extracellular walls, wider at the outside and narrower at the transmembrane regions, forming a mostly low-density funnel structure. Vestibules at the bottom of the funnel are large enough to reserve a sufficient amount of ions for permeation during channel opening. However, the inner Y-shaped density at the top of the vestibule is unique to the $P2X_2$ receptor and is speculated to protect liganded ATP from ATPases. The binding pockets in many ligand-gated channels are distantly located from the transmembrane pore (Miyazawa et al., 2003; Sato et al., 2004). In contrast, the $P2X_2$ receptor interacts with ATP at lysines 69, 71, and 308 proximal to the transmembrane segments (Figure 3A) (Ennion et al., 2000; Jiang et al., 2000). Because negatively charged ATP should be concentrated near the polarized membrane surface, large orifices at the extracellular membrane surface would seem effective for the intake of ATP into the vestibule (Figure 6B). Furthermore, negatively charged ATP would be repulsed toward the outside of the cell upon hyperpolarization of the plasma membrane. As the location of the putative ATP binding pocket is adjacent to the membrane region, it is possible that ATP and its binding site are located within the electric field. This structural feature might result in the voltage dependency of the ATP binding itself and/or that of the conformational change of the binding site with ATP. It is possible that this mechanism underlies the electrophysiologically observed voltage-dependent gating of the $P2X_2$ channels (Nakazawa and Ohno, 2005; Fujiwara et al., 2009).

An activation-dependent increase in permeability, for example pore dilation, is one of the noticeable characteristics of P2X receptors (Khakh et al., 1999; Virginio et al., 1999; Fujiwara and Kubo, 2004). Although it is not yet clear whether this permeability change is caused by a conformational change within the P2X molecule (Fisher et al., 2004) or by the clustering of ATP-liganded P2X receptors, a conformational change at the cytoplasmic C-terminal tips has been suggested from fluorescence resonance energy transfer analysis during pore dilation (Fisher et al., 2004). The structure of the $P2X_2$ receptor reveals a loose association between the constituent subunits, in that contact between subunits is at a limited number of points. This is unusual in ion channels in which the structure has been resolved, and may be one of the bases of the dynamic permeation property of P2X receptors. The structure of the ligand-bound form has yet to be clarified which, when determined, will allow a better understanding of the precise mechanisms of gating and pore dilation of the P2X receptor family.

EXPERIMENTAL PROCEDURES

Expression, Purification, and Cryo-EM of the $P2X_2$ Receptor

N-FLAG $P2X_2$ protein was heterologously expressed in Sf9 cells, solubilized from its membrane using DDM, and purified by immunoaffinity chromatography using anti-FLAG M2 gel (Sigma) followed by Superdex 200 SEC (GE Healthcare) (Mio et al., 2005). $P2X_2$ protein solution (2.5 μl; approximately 0.2 mg/ml) in 20 mM Tris-HCl (pH 7.4), 140 mM NaCl, 5 mM DDM, and 0.02% sodium azide was applied to a preirradiated holey carbon grid, blotted with filter paper, and immediately frozen by plunging it into liquid ethane cooled by liquid nitrogen. The grid was transferred into a JEOL JEM3000SFF

cryo-electron microscope equipped with a helium stage (Fujiyoshi et al., 1991) operated at an acceleration voltage of 300 kV. Images were recorded on Kodak SO163 film at a nominal magnification of 40,400× using low-dose procedures (<20 electrons/Å^2) and at various defocus values fully covering the range between −1.38 and −3.89 μm. Eighty-eight images were digitized with a Scitex Leafscan 45 scanner at a pixel size of 2.48 Å at the specimen level.

For negative staining, purified $P2X_2$ proteins at approximately 50 μg/ml were adsorbed by thin carbon films supported by copper mesh grids which were rendered hydrophilic in advance by glow discharge under low air pressure. The grid surface was washed with five drops of double-distilled water, negatively stained with 2% uranyl acetate solution for 30 s twice, blotted, and dried in air. Micrographs were recorded using a JEOL 100CX transmission electron microscope at 39,000× magnification with 100 kV acceleration voltage.

Automated Particle Selection and 3D Reconstruction

Image analysis was performed using our SPINNS (Yazawa et al., 2007) and the IMAGIC V algorithm (van Heel et al., 1996). The 334 projections of the $P2X_2$ receptor were selected in 140 × 140 pixel subframes from the digitized images by the autoaccumulation method using simulated annealing (Ogura and Sato, 2004a), and used to train a three-layer neural network (NN) auto-picking system (Ogura and Sato, 2004b). From 92,407 particles selected by the NN, false-positive particles, particles containing frost or cracks, and those touching neighboring particles were discarded manually, and after subtracting the uneven background, 90,146 images were analyzed.

Image analysis was performed in three major refinement steps. In the first step, the 90,146 particle images were corrected for the contrast transfer function of the electron microscope (spherical aberration = 1.6 mm, chromatic aberration = 2.2 mm, acceleration voltage = 300 kV) using the defocus values determined with IMAGIC V, and aligned rotationally and translationally (van Heel et al., 1996; Frank, 2006) using the reference free method (Ogura and Sato, 2004b). They were then grouped into 400 clusters using the modified GNG classification algorithm (Ogura et al., 2003). The resulting averages were used as new references, and the cycle from alignment to 2D averaging was repeated 51 times. For the second step, the Euler angles of the class averages were determined by the full automatic 3D reconstruction method using SA (Ogura and Sato, 2006) assuming a C3 symmetry (Mio et al., 2005), and were used to calculate a first 3D structure by the SIRT method (Penczek et al., 1992). The reprojections from the initial volume were employed as references for multireference alignment. Each image in the library was aligned and clustered, providing improved cluster averages, and a new 3D map was generated by the reconstruction method using SA without a 3D reference and reprojected as above. The cycle from reprojection to 3D reconstruction was repeated seven times. For the third step, the 3D map was refined by the projection matching method (Penczek et al., 1994) followed by the echo-correlated reconstruction method for 71 cycles. The final reconstruction included 46,511 particles, 51.6% of all the selected images. The FSC function was used to assess the resolution of the final 3D map. The threshold value used for surface rendering of the density map was contoured at an isosurface containing a volume of 3.933×10^5 Å^3, corresponding to 324.5 kDa, adopting commonly accepted densities of 1.37 g/cm^3 for proteins and for glycan.

SDS Gel Electrophoresis

Samples were mixed with an equal volume of sample buffer containing 62.5 mM Tris-HCl (pH 6.8), 2% SDS, 25% glycerol, 0.04 M dithiothreitol, and 0.01% bromophenol blue, and then incubated at 60°C for 15 min. Proteins were separated in a 2%–15% gradient acrylamide gel and visualized by silver staining. For western blots, electrophoresed proteins were transferred to a PVDF membrane and analyzed with an anti-FLAG antibody (Sigma) and a horseradish peroxidase-labeled secondary antibody. Chemiluminescence was detected using an LAS-3000 mini image analyzer (Fujifilm).

Chemical crosslinking was performed by incubating samples in a buffer containing 5 mM glutaraldehyde at room temperature for 30 min. A Tris buffer component was substituted with phosphate buffer by dialysis in advance. The reaction was terminated by incubation with an equal volume of SDS sample buffer at 60°C for 15 min. The proteins were separated in a 2%–15% acrylamide gel and visualized by silver staining.

For the lectin western blot, aliquots of $P2X_2$ protein treated or not with PNGase F (Sigma) were separated by SDS-PAGE and transferred to the PVDF membrane. The membrane was treated with a biotinylated lectin solution at 4°C for 16 hr, and the bound lectin was detected by alkaline phosphatase-labeled streptavidin. The biotinylated lectins were obtained from Vector Laboratories.

Estimation of Stokes Radius by SEC

The distribution coefficient, *Kav*, was calculated from the equation $Kav = (Ve - V_0)/(Vt - V_0)$, where *Ve* is the elution volume of high molecular weight standards (GE Healthcare) or $P2X_2$ protein. The column void volume (V_0) was measured with blue dextran 2000, and *Vt* represents total bed volume. The Stokes radius (*Rs*) of the $P2X_2$ protein was determined using a calibration curve constructed by plotting the *Rs* of each reference protein versus $(-\log Kav)^{1/2}$ according to the relationship $(-\log Kav)^{1/2} = \alpha\,(\beta + Rs)$ (Laurent and Killander, 1964). All the standards and the $P2X_2$ protein were solubilized in the same buffer used for $P2X_2$ protein purification. The standard proteins used are: thyroglobulin (*Rs* ≈ 85.0 Å), ferritin (61.0 Å), catalase (52.2 Å), and aldolase (48.1 Å). The elution of $P2X_2$ protein was repeated three times; the data are presented by average ± standard deviation (SD).

Decoration of $P2X_2$ Protein with Antibodies or Lectins

Molecular complexes between $P2X_2$ protein and anti-FLAG antibody were generated by mixing the purified $P2X_2$ protein with an anti-FLAG M2 antibody (Sigma) at 4°C for 30 min. After removing excessive antibodies by SEC, the complexes were negatively stained and observed by EM. To obtain clearer images of the $P2X_2$/anti-FLAG antibody complexes, Fab fragments were generated from the antibodies by papain digestion and conjugated with colloidal gold (BB International). The conjugate was isolated from nonreacted Fab molecules by 10%–30% glycerol gradient centrifugation, and then mixed with $P2X_2$ protein at 4°C for 30 min.

For decoration of $P2X_2$ protein with lectin-gold conjugates, $P2X_2$ protein was mixed with ConA- (EY Laboratories) or WGA-gold (BB International) at 4°C for 30 min. After removing the unbound proteins by SEC, the samples were negatively stained.

ACKNOWLEDGMENTS

We thank D. Julius for providing us with $P2X_2$ cDNA, Y. Fujiwara and B. Keceli for discussion, and M. Mio, S. Abe, and M. Yanagihara for technical assistance in biochemistry and image analysis. This work was supported by a Grant-in-Aid for Scientific Research on Priority Areas, Structure of Biological Macromolecular Assemblies to K.M. and C.S., by a grant from the Japan New Energy and Industrial Technology Development Organization (NEDO) to C.S., and by a grant from the Precursory Research for Embryonic Science and Technology (PRESTO) of the Japan Science and Technology Agency to T.O. It was also supported by research grants from the Ministry of Education, Sciences, Sports, Culture and Technology of Japan and from the Japan Society for Promotion of Sciences to Y.K.

Received: September 26, 2008
Revised: November 30, 2008
Accepted: December 2, 2008
Published: February 12, 2009

REFERENCES

Aubert, A., Norris, C.H., and Guth, P.S. (1994). Influence of ATP and ATP agonists on the physiology of the isolated semicircular canal of the frog (*Rana pipiens*). Neuroscience *62*, 963–974.

Barrera, N.P., Ormond, S.J., Henderson, R.M., Murrell-Lagnado, R.D., and Edwardson, J.M. (2005). Atomic force microscopy imaging demonstrates that $P2X_2$ receptors are trimers but that $P2X_6$ receptor subunits do not oligomerize. J. Biol. Chem. *280*, 10759–10765.

Brake, A.J., Wagenbach, M.J., and Julius, D. (1994). New structural motif for ligand-gated ion channels defined by an ionotropic ATP receptor. Nature *371*, 519–523.

Burnstock, G. (2007). Physiology and pathophysiology of purinergic neurotransmission. Physiol. Rev. *87*, 659–797.

Cao, L., Young, M.T., Broomhead, H.E., Fountain, S.J., and North, R.A. (2007). Thr339-to-serine substitution in rat $P2X_2$ receptor second transmembrane domain causes constitutive opening and indicates a gating role for Lys308. J. Neurosci. *27*, 12916–12923.

Cavaliere, F., Florenzano, F., Amadio, S., Fusco, F.R., Viscomi, M.T., D'Ambrosi, N., Vacca, F., Sancesario, G., Bernardi, G., Molinari, M., et al. (2003). Up-regulation of $P2X_2$, $P2X_4$ receptor and ischemic cell death: prevention by P2 antagonists. Neuroscience *120*, 85–98.

Chen, C.C., Akopian, A.N., Sivilotti, L., Colquhoun, D., Burnstock, G., and Wood, J.N. (1995). A P2X purinoceptor expressed by a subset of sensory neurons. Nature *377*, 428–431.

Cockayne, D.A., Dunn, P.M., Zhong, Y., Rong, W., Hamilton, S.G., Knight, G.E., Ruan, H.Z., Ma, B., Yip, P., Nunn, P., et al. (2005). $P2X_2$ knockout mice and $P2X_2/P2X_3$ double knockout mice reveal a role for the $P2X_2$ receptor subunit in mediating multiple sensory effects of ATP. J. Physiol. *567*, 621–639.

Eickhorst, A.N., Berson, A., Cockayne, D., Lester, H.A., and Khakh, B.S. (2002). Control of $P2X_2$ channel permeability by the cytosolic domain. J. Gen. Physiol. *120*, 119–131.

Ennion, S., Hagan, S., and Evans, R.J. (2000). The role of positively charged amino acids in ATP recognition by human $P2X_1$ receptors. J. Biol. Chem. *275*, 29361–29367.

Finger, T.E., Danilova, V., Barrows, J., Bartel, D.L., Vigers, A.J., Stone, L., Hellekant, G., and Kinnamon, S.C. (2005). ATP signaling is crucial for communication from taste buds to gustatory nerves. Science *310*, 1495–1499.

Fisher, J.A., Girdler, G., and Khakh, B.S. (2004). Time-resolved measurement of state-specific $P2X_2$ ion channel cytosolic gating motions. J. Neurosci. *24*, 10475–10487.

Florenzano, F., Viscomi, M.T., Cavaliere, F., Volonte, C., and Molinari, M. (2002). Cerebellar lesion up-regulates $P2X_1$ and $P2X_2$ purinergic receptors in precerebellar nuclei. Neuroscience *115*, 425–434.

Frank, J. (2006). Three-Dimensional Electron Microscopy of Macromolecular Assemblies: Visualization of Biological Molecules in Their Native State (New York: Oxford University Press).

Fujiwara, Y., and Kubo, Y. (2004). Density-dependent changes of the pore properties of the $P2X_2$ receptor channel. J. Physiol. *558*, 31–43.

Fujiwara, Y., Keceli, B., Nakajo, K., and Kubo, Y. (2009). Voltage- and [ATP]-dependent gating of the $P2X_2$ ATP receptor channel. J. Gen. Physiol. *133*, 93–109.

Fujiyoshi, Y., Mizusaki, T., Morikawa, K., Yamagishi, H., Aoki, Y., Kihara, H., and Harada, Y. (1991). Development of a superfluid helium stage for high-resolution electron-microscopy. Ultramicroscopy *38*, 241–251.

Gourine, A.V., Llaudet, E., Dale, N., and Spyer, K.M. (2005). ATP is a mediator of chemosensory transduction in the central nervous system. Nature *436*, 108–111.

Jiang, L.H., Rassendren, F., Surprenant, A., and North, R.A. (2000). Identification of amino acid residues contributing to the ATP-binding site of a purinergic P2X receptor. J. Biol. Chem. *275*, 34190–34196.

Khakh, B.S. (2001). Molecular physiology of P2X receptors and ATP signalling at synapses. Nat. Rev. Neurosci. *2*, 165–174.

Khakh, B.S., Bao, X.R., Labarca, C., and Lester, H.A. (1999). Neuronal P2X transmitter-gated cation channels change their ion selectivity in seconds. Nat. Neurosci. *2*, 322–330.

Khakh, B.S., Zhou, X., Sydes, J., Galligan, J.J., and Lester, H.A. (2000). State-dependent cross-inhibition between transmitter-gated cation channels. Nature *406*, 405–410.

Laurent, T.C., and Killander, J. (1964). A theory of gel filtration and its experimental verification. J. Chromatogr. *14*, 317–330.

Lewis, C., Neidhart, S., Holy, C., North, R.A., Buell, G., and Surprenant, A. (1995). Coexpression of $P2X_2$ and $P2X_3$ receptor subunits can account for ATP-gated currents in sensory neurons. Nature *377*, 432–435.

Long, S.B., Campbell, E.B., and Mackinnon, R. (2005). Crystal structure of a mammalian voltage-dependent Shaker family K^+ channel. Science *309*, 897–903.

Migita, K., Haines, W.R., Voigt, M.M., and Egan, T.M. (2001). Polar residues of the second transmembrane domain influence cation permeability of the ATP-gated $P2X_2$ receptor. J. Biol. Chem. *276*, 30934–30941.

Mio, K., Kubo, Y., Ogura, T., Yamamoto, T., and Sato, C. (2005). Visualization of the trimeric $P2X_2$ receptor with a crown-capped extracellular domain. Biochem. Biophys. Res. Commun. *337*, 998–1005.

Mio, K., Ogura, T., Kiyonaka, S., Hiroaki, Y., Tanimura, Y., Fujiyoshi, Y., Mori, Y., and Sato, C. (2007). The TRPC3 channel has a large internal chamber surrounded by signal sensing antennas. J. Mol. Biol. *367*, 373–383.

Miyazawa, A., Fujiyoshi, Y., and Unwin, N. (2003). Structure and gating mechanism of the acetylcholine receptor pore. Nature *423*, 949–955.

Nakagawa, T., Cheng, Y., Ramm, E., Sheng, M., and Walz, T. (2005). Structure and different conformational states of native AMPA receptor complexes. Nature *433*, 545–549.

Nakazawa, K., and Ohno, Y. (2005). Characterization of voltage-dependent gating of $P2X_2$ receptor/channel. Eur. J. Pharmacol. *508*, 23–30.

Nakazawa, K., Yamakoshi, Y., Tsuchiya, T., and Ohno, Y. (2005). Purification and aqueous phase atomic force microscopic observation of recombinant $P2X_2$ receptor. Eur. J. Pharmacol. *518*, 107–110.

Newbolt, A., Stoop, R., Virginio, C., Surprenant, A., North, R.A., Buell, G., and Rassendren, F. (1998). Membrane topology of an ATP-gated ion channel (P2X receptor). J. Biol. Chem. *273*, 15177–15182.

North, R.A. (2002). Molecular physiology of P2X receptors. Physiol. Rev. *82*, 1013–1067.

Ogura, T., and Sato, C. (2001). An automatic particle pickup method using a neural network applicable to low-contrast electron micrographs. J. Struct. Biol. *136*, 227–238.

Ogura, T., and Sato, C. (2004a). Auto-accumulation method using simulated annealing enables fully automatic particle pickup completely free from a matching template or learning data. J. Struct. Biol. *146*, 344–358.

Ogura, T., and Sato, C. (2004b). Automatic particle pickup method using a neural network has high accuracy by applying an initial weight derived from eigenimages: a new reference free method for single-particle analysis. J. Struct. Biol. *145*, 63–75.

Ogura, T., and Sato, C. (2006). A fully automatic 3D reconstruction method using simulated annealing enables accurate posterioric angular assignment of protein projections. J. Struct. Biol. *156*, 371–386.

Ogura, T., Iwasaki, K., and Sato, C. (2003). Topology representing network enables highly accurate classification of protein images taken by cryo electron-microscope without masking. J. Struct. Biol. *143*, 185–200.

Penczek, P., Radermacher, M., and Frank, J. (1992). Three-dimensional reconstruction of single particles embedded in ice. Ultramicroscopy *40*, 33–53.

Penczek, P.A., Grassucci, R.A., and Frank, J. (1994). The ribosome at improved resolution: new techniques for merging and orientation refinement in 3D cryo-electron microscopy of biological particles. Ultramicroscopy *53*, 251–270.

Rosenthal, P.B., and Henderson, R. (2003). Optimal determination of particle orientation, absolute hand, and contrast loss in single-particle electron cryomicroscopy. J. Mol. Biol. *333*, 721–745.

Sato, C., Ueno, Y., Asai, K., Takahashi, K., Sato, M., Engel, A., and Fujiyoshi, Y. (2001). The voltage-sensitive sodium channel is a bell-shaped molecule with several cavities. Nature *409*, 1047–1051.

Sato, C., Hamada, K., Ogura, T., Miyazawa, A., Iwasaki, K., Hiroaki, Y., Tani, K., Terauchi, A., Fujiyoshi, Y., and Mikoshiba, K. (2004). Inositol 1,4,5-trisphosphate receptor contains multiple cavities and L-shaped ligand-binding domains. J. Mol. Biol. *336*, 155–164.

Tichelaar, W., Safferling, M., Keinanen, K., Stark, H., and Madden, D.R. (2004). The three-dimensional structure of an ionotropic glutamate receptor reveals a dimer-of-dimers assembly. J. Mol. Biol. *344*, 435–442.

Torres, G.E., Egan, T.M., and Voigt, M.M. (1998). Topological analysis of the ATP-gated ionotropic $P2X_2$ receptor subunit. FEBS Lett. *425*, 19–23.

Torres, G.E., Egan, T.M., and Voigt, M.M. (1999). Identification of a domain involved in ATP-gated ionotropic receptor subunit assembly. J. Biol. Chem. *274*, 22359–22365.

Tsuda, M., Shigemoto-Mogami, Y., Koizumi, S., Mizokoshi, A., Kohsaka, S., Salter, M.W., and Inoue, K. (2003). $P2X_4$ receptors induced in spinal microglia gate tactile allodynia after nerve injury. Nature *424*, 778–783.

Unwin, N. (2005). Refined structure of the nicotinic acetylcholine receptor at 4 Å resolution. J. Mol. Biol. *346*, 967–989.

Valera, S., Hussy, N., Evans, R.J., Adami, N., North, R.A., Surprenant, A., and Buell, G. (1994). A new class of ligand-gated ion channel defined by P2X receptor for extracellular ATP. Nature *371*, 516–519.

van Heel, M., Harauz, G., Orlova, E.V., Schmidt, R., and Schatz, M. (1996). A new generation of the IMAGIC image processing system. J. Struct. Biol. *116*, 17–24.

van Heel, M., Gowen, B., Matadeen, R., Orlova, E.V., Finn, R., Pape, T., Cohen, D., Stark, H., Schmidt, R., Schatz, M., et al. (2000). Single-particle electron cryo-microscopy: towards atomic resolution. Q. Rev. Biophys. *33*, 307–369.

Virginio, C., MacKenzie, A., Rassendren, F.A., North, R.A., and Surprenant, A. (1999). Pore dilation of neuronal P2X receptor channels. Nat. Neurosci. *2*, 315–321.

Yazawa, M., Ferrante, C., Feng, J., Mio, K., Ogura, T., Zhang, M., Lin, P.H., Pan, Z., Komazaki, S., Kato, K., et al. (2007). TRIC channels are essential for Ca^{2+} handling in intracellular stores. Nature *448*, 78–82.

